Title
Use of polar decomposition for the diagnosis of oral precancer.

Journal
Applied Optics, 46(15)

ISSN
1559-128X

Authors
Chung, Jungrae
Jung, Woonggyu
Hammer-Wilson, Marie J
et al.

Publication Date
2007-05-20

DOI
10.1364/ao.46.003038

Use of polar decomposition for the diagnosis of oral precancer

Jungrae Chung, Woonggyu Jung, Marie J. Hammer-Wilson, Petra Wilder-Smith, and Zhongping Chen

The Mueller matrix describes all the polarizing properties of a sample and, therefore, the optical differences between noncancerous and precancerous tissue that may be present within the matrix elements. A high-speed polarimetry system that generates 16 (4×4) full Mueller matrices to characterize tissues is presented. Feature extraction is done on the Mueller matrix elements resulting in depolarization and retardance images by polar decomposition. These are used to detect and classify early oral cancers and precancerous changes in epithelium such as dysplasia. These images are compared with orthogonal polarization images and analyzed in an attempt to identity useful factors for the differentiation between cancerous lesions and their benign counterparts. Our results indicate that polarimetry has potential as a method for the *in vivo* early detection and diagnosis of oral premalignancy.

OCIS codes: 230.0230, 170.3890, 230.5440, 290.7050.

1. Introduction

An estimated 1,444,920 new cases of cancer will be diagnosed in the United States in the year 2007, and an estimated 559,650 Americans will die from cancer.[1] Cancer (190.1 per 100,000) was the second leading cause of death in the United States in the year 2003, exceeded only by heart disease (231.6 per 100,000).[1] More than 85% of cancers originate in the epithelium, and epithelial cancers are preceded by a curable precancerous stage. As such, early detection is paramount for the successful treatment of this disease. If detected at precancerous stage, 95% of the cases have a complete recovery.[2] However, many forms of precancerous changes are difficult to detect using conventional techniques, which require histological examination of biopsies obtained from visible lesions or random surveillance biopsies.

Biological tissues are optically inhomogeneous, birefringent, and absorbing media.[3] Precancerous lesions are characterized by increased nuclear size and nuclear and/or cytoplasmic ratio. The scattering from the epithelial layer of tissue can provide information on nuclear morphology.[4] The rate of depolarization of incident polarized light depends on the morphological and optical features such as the density, size, shape, and refractive index in the tissue.[5] Cancerous tissues depolarize light less than their surrounding tissues do, whereas noncancerous tissues have the same depolarizing properties as the surrounding tissue.[6]

This effect is caused by changes in the subsurface structures of cancerous tissues that prevent light from penetrating the tissue as deeply as it would in normal tissue. These facts support an optical approach to noninvasive cancer detection.

In the field of optical imaging, there are a number of subsurface imaging techniques such as optical coherence tomography,[7] linear and nonlinear emission and harmonic generation imaging,[8,9] and confocal microscopy.[10] These techniques provide high resolution images of subsurface structures with the drawback that the imaging depth is small (i.e., 1 to 2 mm or less). To provide larger imaging depths, other techniques need to be explored. The imaging depth into the tissue depends on the scattering and absorption characteristic of the tissue. Demos and Alfano[11] showed that the spectral polarization differences imaging techniques (SPDI) was an imaging tool that can provide subsurface imaging at larger depth, and deep surface

The authors are all with the Beckman Laser Institute, University of California, Irvine, California 92612, USA. W. Jung and Z. Chen are also with the university's Department of Biomedical Engineering. J. Chung's e-mail address is jrchung@uci.edu.

Received 29 June 2006; revised 13 December 2006; accepted 5 January 2007; posted 9 January 2007 (Doc. ID 72443); published 1 May 2007.

0003-6935/07/153038-08$15.00/0

imaging in tissue (1.5 cm beneath the surface) was demonstrated by using both spectral and polarization discrimination of the backscattered photons.[12]

In 1976, Bickel *et al.*[13] advanced polarimetry into the field of biomedical sensing when they described a technique that measured the polarization effects of the scattered light from bacterial suspensions to yield useful information to characterize the sample. In the ensuing decades, several groups have shown that a considerable amount of information, such as the average particle size,[14] photon path length,[15] and particle shape[16–18] can be obtained from polarization sensitive measurements of the sample under investigation.[19] In addition, others have shown that polarization-based imaging measurements can provide enhanced visualization of superficial structures[20–22] to allow for subsurface imaging.[23] The aforementioned applications of polarimetry for biomedical imaging involve the use of Mueller–Stokes calculus to mathematically depict how a biological sample affects the polarization vector of an incident light beam, determined by either backscattered[14,15,24,25] or transmitted[26–28] light intensities from the sample. The experimental Mueller matrix of a sample contains information on retardance, diattenuation, and depolarization, which is not readily apparent in the original images. These sample discriminating parameters can be extracted using polar decomposition. The decomposition of Mueller matrices into a combination of product matrices has been addressed by many authors.[29–32] Lu and Chipman[29] were able to decompose the Mueller matrix into three factors, namely, diattenuation, retardance, and depolarization. Several groups have developed a Mueller matrix imaging polarimeter capable of collecting the full Mueller matrix of tissue *in vivo*.[3,33] They have shown that by matrix decomposition the retardance and depolarization parameters show potential for distinguishing between varieties of dermatological conditions including malignant moles. A system similar to that presented here has been previously reported in a publication in 2002.[34] However, that system did not have enough resolution to allow analysis of celluar and nuclear morphologic features of tissue sections. To the best of our knowledge, no research has been performed to correlate the observed changes in the Mueller matrix to the changes in the tissue structure that occur as the tissue becomes precancerous. The main innovations in this current system are the histologic-quality images of cell morphology obtained by using objective lens and the better acquisition time to obtain the Mueller matrices. This system is capable of collecting the Mueller matrix, and the time taken to do so would be much less than 15 s. The basis for the optical detection of a precancerous stage, such as dysplasia, is the exploitation of pathology related changes in the optical properties of the tissue.[35] We hypothesize that it is through the observation of these morphologic and biochemical changes that precancerous tissue can be distinguished from noncancerous tissue. These images are compared with the orthogonal polarization image and analyzed in an attempt to determine specific diagnostic criteria for the identification of cancerous lesions from their benign counterparts. Our results indicate that polarimetry has potential as a method for the *in vivo* early detection and diagnosis of oral premalignancy.

2. Theory

A. Stokes Vector and Mueller Matrix

In 1943, Hans Mueller developed a matrix that relates the Stokes vector of the light impinging on a sample to the Stokes vector leaving sample models.[36] Using the method with the input and output polarization states (Stokes vectors) known, the 4×4 Mueller matrix can be used to describe the polarization properties of a sample. This relationship is shown below in Eq. (1), where M_{sample} is the Mueller matrix of a sample and S_{out} and S_{in} are the output and input Stokes vectors respectively:

$$S_{out} = \begin{bmatrix} S_0 \\ S_1 \\ S_2 \\ S_3 \end{bmatrix}_{out} = \begin{bmatrix} M_{00} & M_{01} & M_{02} & M_{03} \\ M_{10} & M_{11} & M_{12} & M_{13} \\ M_{20} & M_{21} & M_{22} & M_{23} \\ M_{30} & M_{31} & M_{32} & M_{33} \end{bmatrix}_{sample} \begin{bmatrix} S_0 \\ S_1 \\ S_2 \\ S_3 \end{bmatrix}_{in}. \quad (1)$$

The Stokes parameters S consist of four values. The first parameter, S_0, is simply the overall intensity of the light. The second parameter, S_1, is the tendency of the light to exhibit either a horizontal ($S_1 > 0$) or a vertical ($S_1 < 0$) polarization state. Similary, the third parameter, S_2, is the tendency of the light to exhibit either a $+45°$ ($S_2 > 0$) or a $-45°$ ($S_2 < 0$) polarization state. Finally, the fourth parameter, S_3, is the tendency of the light to exhibit either a right ($S_3 > 0$) or a left ($S_3 < 0$) polarization state. The value for a specific Stokes parameter will be zero if neither of the states for a given parameter is observed.

For simplicity, a Mueller matrix is normalized by dividing all the M_{ij} elements by the M_{00} element. The resulting normalized matrix has an M_{00} element that is identically $+1$ and the remaining elements range from -1 to $+1$. For a given sample, a Mueller matrix M can be accomplished with 16 polarization images, as depicted in Table 1.

We calculate orthogonal polarization images (I_{OP}) by using[3]

$$I_{OP} = \frac{I_{par} - I_{per}}{I_{par} + I_{per}}, \quad (2)$$

where I_{par} is the image at light with the polarizer oriented to accept light parallel to the incident light, and I_{per} is the image at light with the polarizer oriented to accept light perpendicular to the incident light.

B. Decomposition for Depolarizing Mueller Matrices

A practical method of categorizing Mueller matrices M is by describing the type of polarization element that is represented. The three polarization properties are retardance, diattenuation, and depolarization.

Table 1. Calculation of the 16 Full Mueller Matrix[a]

M_{00} = HH + HV + VH + VV	M_{01} = HH + HV − VH − VV	M_{02} = 2PH + 2PV − M_{00}	M_{03} = 2RH + 2RV − M_{00}
M_{10} = HH − HV + VH − VV	M_{11} = HH − HV − VH + VV	M_{12} = 2PH − 2PV − M_{10}	M_{13} = 2RH − 2RV − M_{10}
M_{20} = 2HP + 2VP − M_{00}	M_{21} = 2HP − 2VP − M_{01}	M_{22} = 4PP − 2PH − 2PV − M_{20}	M_{23} = 4RP − 2RH − 2RV − M_{20}
M_{30} = 2HR + 2VR − M_{00}	M_{31} = 2HR − 2VR − M_{01}	M_{32} = 4PR − 2PH − 2PV − M_{30}	M_{33} = 4RR − 2RH − 2RV − M_{30}

[a]The notation is as follows: the first term represents the input polarization state, and the second term represents the output polarization state. The states are defined as: H for horizontal, V for vertical, P for +45°, and R for right circular.

There are 16° of freedom in the Mueller matrix: one in intensity (transmittance, reflectance, scattering), three in retardance, three in diattenuation, and nine in depolarization. An object's Mueller matrix may contain any combination of these properties, which are extracted by using a polar decomposition process. This polar decomposition, explained in detail by Lu and Chipman,[37] separates the Mueller matrix into three 4×4 matrices: the depolarization matrix M_Δ, the retarding matrix M_R, and the diattenuation matrix M_D. A brief description of the theory is presented here. Let M be a depolarizing Mueller matrix. M can be decomposed as

$$M = M_\Delta \times M_R \times M_D. \tag{3}$$

Diattenuation D can be acquired directly through the algebraic calculation of the elements in the Muller matrix shown by

$$D = \frac{\sqrt{{m_{01}}^2 + {m_{02}}^2 + {m_{03}}^2}}{m_{00}}. \tag{4}$$

The Mueller matrix for a diattenuator with a diattenuator vector $\bar{D}$ is

$$M_D = T_u \begin{bmatrix} 1 & \bar{D}^T \\ \bar{D} & m_D \end{bmatrix}, \tag{5}$$

$$m_D = \sqrt{1 - D^2} I + \left(1 - \sqrt{1 - D^2}\right) \hat{D}\hat{D}^T, \tag{6}$$

in which I is the 3×3 identity matrix, m_D is the 3×3 submatrix of M_D, $\bar{D}$ is the diattenuation vector, T_u is a transmittance for unpolarized light, and $\hat{D}(= \bar{D}/D)$ denotes the unit vector along $\bar{D}$:

$$T_u = m_{00}, \qquad \bar{D} = \frac{1}{m_{00}} \begin{bmatrix} m_{01} \\ m_{02} \\ m_{03} \end{bmatrix}. \tag{7}$$

Define a three-by-three submatrix m of M by striking out the first row and the first column of M:

$$m \equiv \frac{1}{m_{00}} \begin{bmatrix} m_{11} & m_{12} & m_{13} \\ m_{21} & m_{22} & m_{23} \\ m_{31} & m_{32} & m_{33} \end{bmatrix}, \tag{8}$$

then M can be written as

$$M = m_{00} \begin{bmatrix} 1 & \bar{D}^T \\ \bar{P} & m \end{bmatrix}, \tag{9}$$

in which $\bar{D}$ and $\bar{P}$ are the diattenuation and polarizance vectors of M. Define a Mueller matrix M' based upon M as

$$M' \equiv M {M_D}^{-1}. \tag{10}$$

Note that M' has no diattenuation. However, M' is not a pure retarder as in the case of a nondepolarizing element because M' contains both retardance and depolarization. M' is then further decomposed as a depolarizer followed by a retarder, i.e.,

$$M' = M_\Delta M_R = \begin{bmatrix} 1 & \bar{0}^T \\ \bar{P}_\Delta & m_\Delta \end{bmatrix} \begin{bmatrix} 1 & \bar{0}^T \\ \bar{0} & m_R \end{bmatrix} = \begin{bmatrix} 1 & \bar{0}^T \\ \bar{P}_\Delta & m_\Delta m_R \end{bmatrix} = \begin{bmatrix} 1 & \bar{0}^T \\ \bar{P}_\Delta & m' \end{bmatrix}. \tag{11}$$

Equations (9) and (10) lead to

$$\bar{P}_\Delta = \frac{\bar{P} - m\bar{D}}{1 - D^2}, \tag{12}$$

$$m' = m_\Delta m_R. \tag{13}$$

The four-by-four matrix decomposition reduces to a three-by-three matrix decomposition given Eq. (12). Actually this is equivalent to the polar decomposition of a three-by-three real matrix. Equation (12) leads to

$${m_\Delta}^2 = m'(m')^T. \tag{14}$$

Let λ_1, λ_2, and λ_3 be eigenvalues of $m'(m')^T$. From Eq. (14) it follows that m_Δ has $\sqrt{\lambda_1}$, $\sqrt{\lambda_2}$, and $\sqrt{\lambda_3}$ as eigenvalues, assuming that m' is nonsingular. Applying the Cayley–Hamilton theorem and Eq. (14), m_Δ can be obtained by

$$m_\Delta = \pm \left\{ m'(m')^T + \left(\sqrt{\lambda_1\lambda_2} + \sqrt{\lambda_2\lambda_3} + \sqrt{\lambda_3\lambda_1}\right) I \right\}^{-1} \times \left\{ \left(\sqrt{\lambda_1} + \sqrt{\lambda_2} + \sqrt{\lambda_3}\right) m'(m')^T + \sqrt{\lambda_1\lambda_2\lambda_3} I \right\}. \tag{15}$$

If the determinant of m' is negative then the minus sign is applied. Otherwise the plus sign is applied.

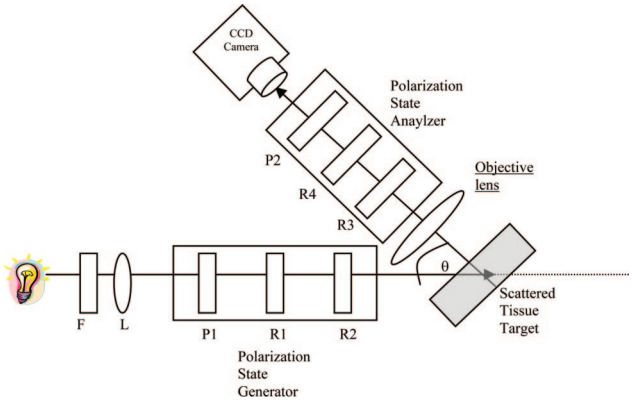

Fig. 1. (Color online) Mueller matrix polarimetry system.

Then the submatrix m_R of retardance matrix M_R can be obtained by

$$m_R = m_\Delta{}^{-1} m'. \tag{16}$$

Its depolarization power denoted by Δ is given by

$$\Delta = 1 - \frac{|trace(m_\Delta)|}{3}, \quad 0 \le \Delta \le 1. \tag{17}$$

Last, the retardance matrix M_R can be known and the retardance can be acquired by

$$R = \cos^{-1}\left[\frac{trace(M_R)}{2} - 1\right]. \tag{18}$$

3. Materials and Methods

A. Experimental Setup

The system shown in Fig. 1 consists of four voltage-controlled optical elements (Meadowlark Optics, Frederick, Colo.). The system light source is a fiber optic illuminator (Dolan-Jenner Industries, Inc., Lawrence, Mass.) with a 30 W, 20 V halogen bulb. The light is passed through a laser line interference filter with wavelength transmittance from 400 to 700 nm. The light emerging from the filter is collimated with a 38.1 mm focal length convex lens (Newport Corporation, Fountain Valley, Calif.) to provide a broad beam to illuminate the sample. The resulting light is then passed through a Glans Thompson 100,000:1 polarizer (Newport Corporation, Fountain Valley, Calif.), a linear polarizer set at horizontal, and two voltage-controlled variable retarders. These optical components allow for modulation of the input state of polarization. The variable retarders produce all the necessary states of linearly and circularly polarized light. The operational basis underlying voltage-controlled optics is that voltage supplied in

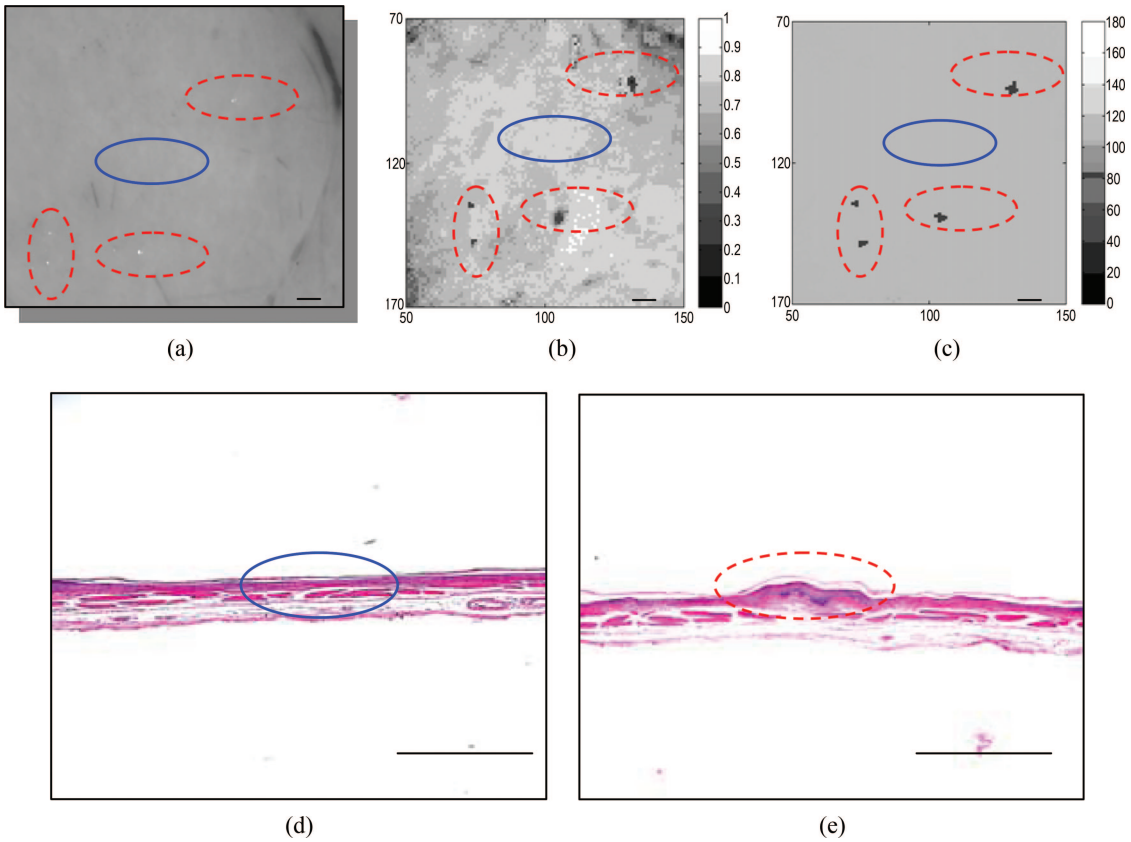

Fig. 2. (Color online) (a) *In situ* Microscopic image of hamster cheek pouch tissue with precancer. Dysplasia and normal region are marked by the dotted circles and the lined circles, respectively, (b) 2D depolarization image, (c) 2D retardance image. Scare bars, 1 mm. (d) Histology in the healthy tissue and (e) histology in the dysplastic region. Scale bars, 0.5 mm.

the form of a 2 kHz square wave modulates the degree of rotation of the polarization axis and the amount of retardation by the voltage controlled retarder. After scattering by the sample, light scattered in the direction of the camera passes through another series of polarizing optics. The backscattered light from the tissue is imaged by the objective lens (10×/0.30 N.A.). The theoretical resolution of this objective [λ/(2*N.A.)] is approximately 0.7–1.2 μm. Before, the resolution was approximately 15–20 μm. The calibrated resolution is approximately 1.5–2.0 μm. The output branch contains another polarizer set at vertical, consisting of two voltage-controlled variable retarders encountered by the light in reverse order from the input branch. The resulting images are captured with a computer controlled 1024 × 1024 pixels, 14 μm × 14 μm per pixel, and 12 bit CCD camera (Kodak, San Diego, Calif.).

B. Animal Model Preparation

1. *Tumor Induction*

A total of nine cheek pouches in female golden Syrian hamsters (Mesocricetus auratus) were used for *in vivo* imaging.[38] Application of 0.5% DMBA (9, 10 dimethyl-1, 2-benzanthracene) in mineral oil three times per week produced mild to severe dysplasia after 3–6 weeks that progressed to squamous cell carcinoma at approximately 10 weeks. The right cheek pouch of each hamster was treated with DMBA carcinogen in mineral oil; the other cheek pouch was treated only with mineral oil. Previous studies have shown that the carcinogenesis process in one cheek pouch does not affect the other cheek. Therefore the treated cheek pouch does not affect the other cheek.[39,40] The histological features in this model have been shown to correspond closely with those of premalignancy and malignancy in human oral mucosa.[38]

2. *Imaging*

Five hamsters were anesthetized using intraperitoneal 2:1 Ketamine HCL (100 mg/ml): Xylazine (20 mg/ml) at a dose of 0.75 cc/kg. These animals were then wrapped in mylar with a cotton oversleeve to prevent hypothermia. The cheek pouches were everted, held in place with a tension clamp, kept moist by irrigation with normal saline, and imaged

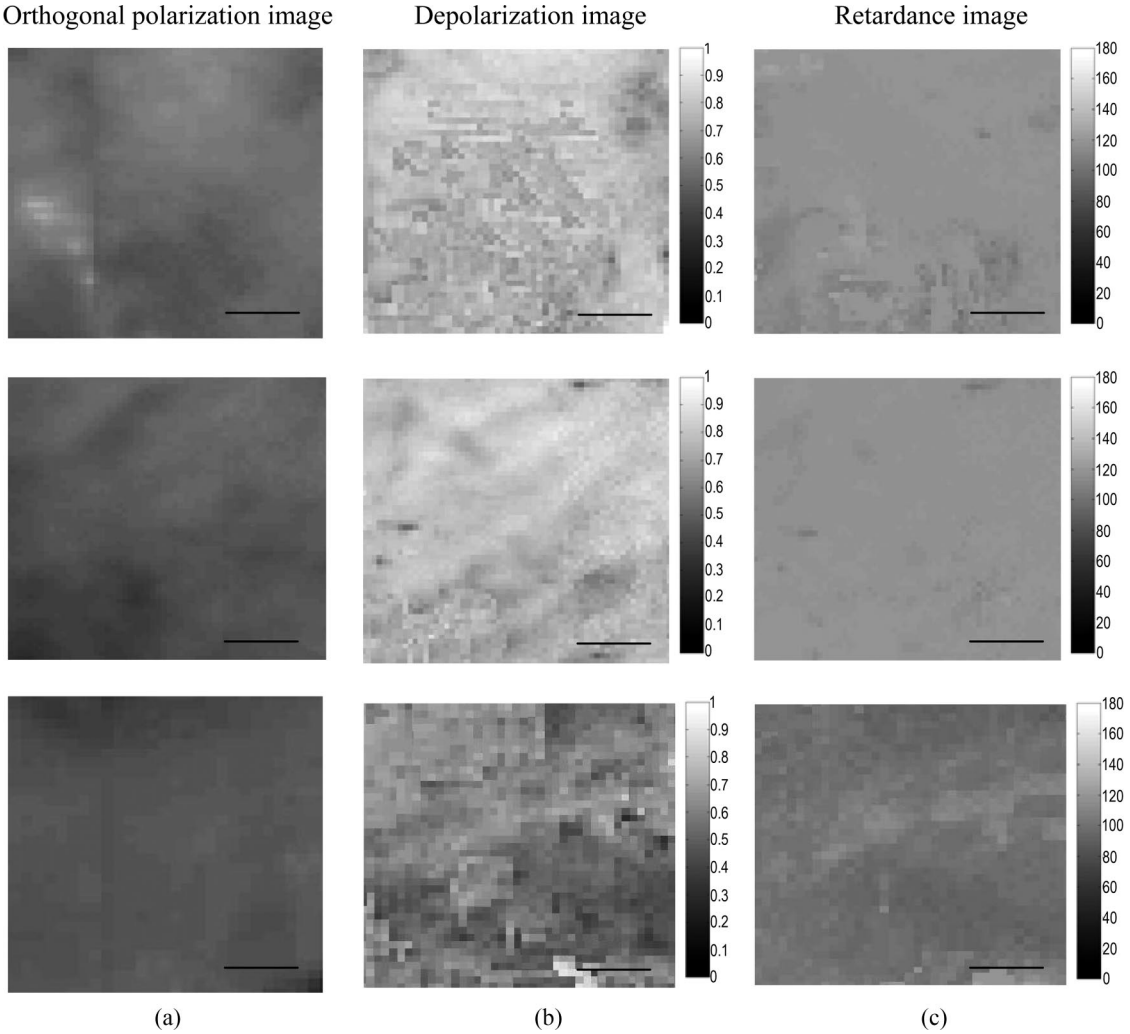

Fig. 3. (a) Orthogonal polarization images, (b) depolarization images, and (c) retardance images for the M_{33} element of the Mueller matrix of healthy tissues. The scale bars are 0.5 mm.

in vivo in near real time. In some animals, imaging at the same location was performed twice to provide an indication of image fidelity. Immediately after imaging, the hamsters were euthanized and the specimens excised for histologic preparation.

Four specimens for *in situ* dysplasia and tumor imaging were obtained from four hamsters. The hamsters were euthanized and each cheek pouch was carefully dissected out and pinned onto a corkboard using 0.20 mm inset pins. The tissues were imaged immediately after positioning. The samples were then fixed and sent for histological processing.

The animals used in this study were housed and treated in accordance with animal research committee guidelines at the University of California, Irvine (approval number 1997-1972).

C. Histology

After imaging the tissue was formalin fixed, photographed through a steromicroscope for gross visual documentation, and then processed for paraffin embedding. Several 6 μm paraffin sections were cut and Hematoxylin and eosin (H&E) stained. The polarization images for each tissue sample were compared with the corresponding steromicrographs for orientation and identification of the imaged area. The histologic sections taken from the imaged areas were examined using standard light microscopy to determine the degree of pathology present.

4. Results

Hamster oral mucosa was imaged at all stages of carcinogenesis in the hamster cheek pouch model. Panel (a) in Fig. 2 presents an *in situ* microscopic image of hamster cheek pouch tissue with precancer. The dysplastic and normal regions are marked by red and blue dotted circles, respectively. The 2D polarization and 2D retardance images for both normal and cancerous regions are shown in Figs. 2(b) and 2(c), respectively. Figures 2(d) and 2(e) show the histology of normal and dysplastic regions, respectively. As theses figures show, depolarization and retardance images can be used to quantitatively identify the dysplastic region of tissue. These advances in

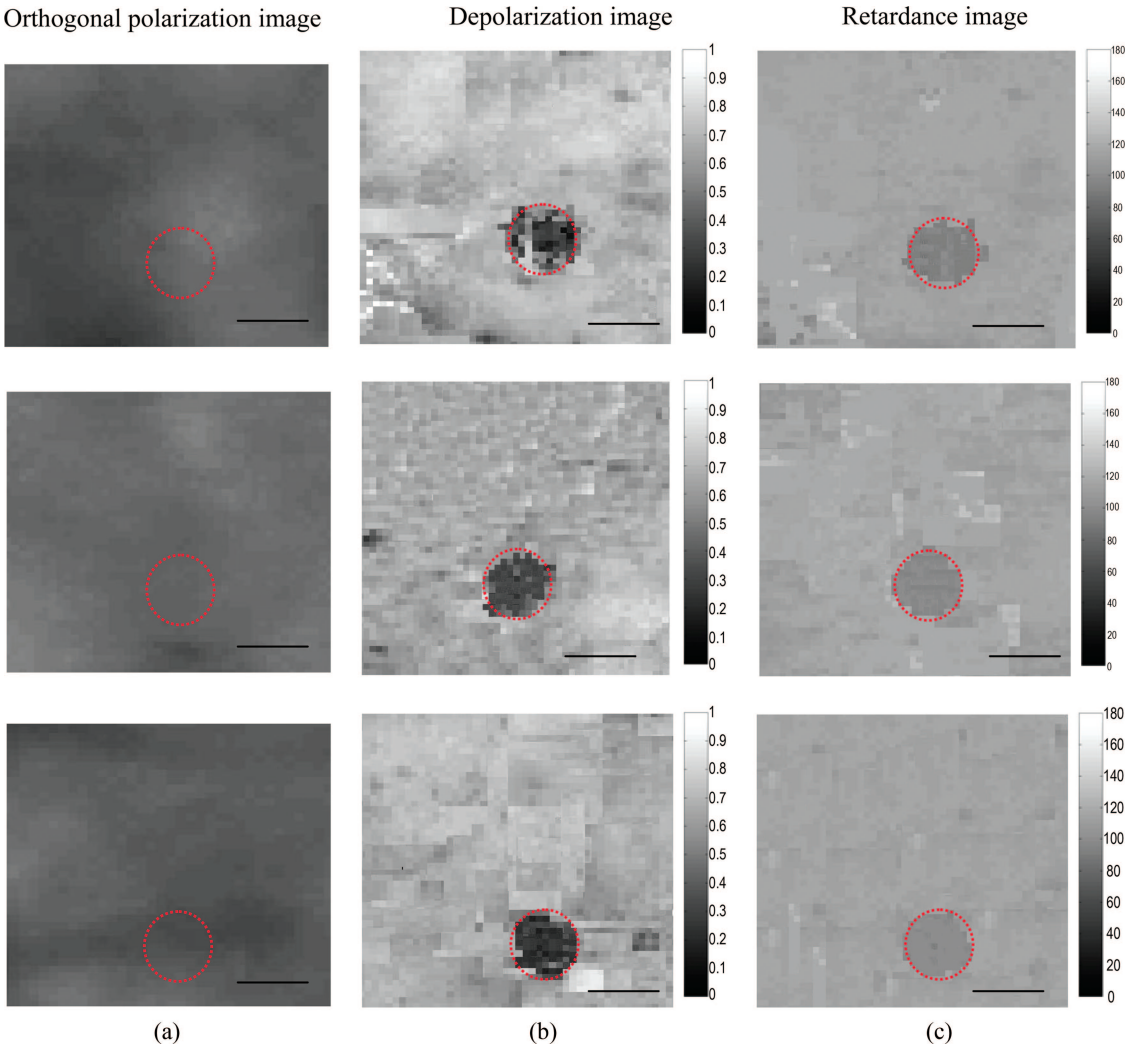

Fig. 4. (Color online) (a) Orthogonal polarization images, (b) depolarization images, and (c) retardance images for the M_{33} element of the Mueller matrix of precancerous tissues. The scale bars are 0.5 mm.

depolarization and retardance imaging promise ultimately to permit earlier and more sensitive diagnosis and to improve the monitoring of disease progression, the identification of region margins, and the assessment of cancer response to therapy.

Figures 3 and 4 depict the orthogonal polarization, depolarization, and retardance images *in vivo* for normal and precancerous tissues, respectively. These images were from three different hamster cheek pouches and the imaged fields were 2.25 mm $\times$ 2.25 mm. Based on the polarization images, the Mueller matrix images were reconstructed, decomposed, and compared with orthogonal polarization images. Figures 3(a) and 4(a) are the orthogonal, polarization images (I_{OP}) for healthy and precancerous tissues, respectively, and no noticeable differences between them are apparent.

Depolarization describes the process of how polarized light can be converted into light with a lower degree of polarization. Depolarization can be the result of a disordered medium or scattering from the surface. One quantity that describes the depolarizing behavior of an element is the depolarization index (Δ). The depolarization index of a Mueller matrix can range from 1 for a perfect depolarizer to 0 for completely polarized light. Based on the data presented in Figs. 3(b) and 4(b), depolarization properties may be useful for differentiating between healthy and precancerous tissues, as precancerous tissue depolarizes light less than healthy tissue.

The greatest variation in retardance values was seen in the M_{33} element of the Mueller matrix, which describes the circular retardance characteristic of a sample. Only the M_{33} element of the Mueller matrix is presented along with the associated retardance image for healthy and precancerous tissues in Figs. 3(c) and 4(c). It indicates that retardance values change within the precancerous lesion, while no change is visible for the noncancerous tissues. These individual pixel value changes result in a lower average retardance value for precancerous tissues. These depolarization and retardance images are potentially useful not only for differentiating between samples but also for boundary identification.

5. Discussion and Conclusion

We have demonstrated the use of polarization for early detection and diagnosis of oral precancer. The fact that our system can be used for tissue characterization suggests its potential application as a noninvasive modality for the detection and monitoring of precancer and suspicious oral tissue lesions. A Mueller matrix is extremely powerful because it completely describes the polarization altering properties of a sample; however, a raw Mueller matrix is difficult to interpret and provides little physical insight. As such, polar decomposition of the Mueller matrix was performed to yield the more familiar quantities of retardance (birefringence), diattenuation (dichroism), and depolarization. It was shown that there is some measurable depolarization to differentiate between noncancerous and precancerous lesions. Therefore precancerous lesions depolarize light less than healthy tissue, and noncancerous lesions depolarize the light the same as the surrounding tissue. Finally, it indicates that the retardance value changes within the precancerous lesion, while no change is visible for the healthy lesion. These individual pixel value changes result in a lower average retardance value for the cancerous sample. These depolarization and retardance images are potentially useful not only for differentiating between samples but also for boundary identification.

The authors thank David S. Mukai, Naglaa El-Abbadi, Nevine Hanna, Teri Waite-Kennedy, and Tanya Burney for their help with animal preparation, regulatory compliance, and sample processing. This work was supported by research grants awarded from the National Science Foundation (BES-86924), the California Tobacco Related Disease Research Program (14IT-0097), and National Institutes of Health (EB-00293, NCI-91717, RR-01192, EB0002SS, EB002494, and AR47551). Institute support from the Air Force Office of Scientific Research (F49620-00-1-0371, FA9550-04-1-0101), Cancer Research Foundation of America (CRFA 30003), California Cancer Research Program (CCRP 00-01391V-20235), and the Beckman Laser Institute Endowment is also acknowledged.

References

1. http://www.cancer.org/downloads/STT/CAFF2007PWSecured.pdf.
2. NIH-National Cancer Institute, *What You Need To Know About Skin Cancer,* NIH Publication No. 95-1564 (1995).
3. S. L. Jacques, J. R. Roman, and K. Lee, "Imaging superficial tissue with polarized light," Lasers Surg. Med. **26,** 119–129 (2000).
4. K. Sokolov, R. A. Drezek, K. Gossage, and R. R. Richards-Kortum, "Reflectance spectroscopy with polarized light: Is it sensitive to cellular and nuclear morphology," Opt. Express **5,** 302–317 (1999).
5. J. R. Mourant, T. M. Johnson, S. Carpenter, A. Guerra, T. Aida, and J. P. Freyer, "Polarized angular dependent spectroscopy of epithelial cells and epithelial cell nuclei to determine the size scale of scattering structures," J. Biomed. Opt. **7,** 378–387 (2002).
6. M. H. Smith, "Interpreting Mueller matrix images of tissues," in Proc. SPIE **4257,** 82–89 (2001).
7. D. Huang, E. A. Swanson, C. P. Lin, J. S. Schuman, W. G. Stinson, W. Chang, W. M. R. Hee, T. Flotte, K. Gregory, C. A. Puliafito, and J. G. Fujimoto, "Optical coherence tomography," Science **254,** 1178–1181 (1991).
8. W. Denk, J. H. Strickler, and W. W. Webb, "2-photon laser scanning fluorescence microscopy," Science **248,** 73–76 (1990).
9. Y. C. Guo, P. P. Ho, H. Savage, D. Harris, P. Sacks, S. Schantz, F. Liu, N. Zhadin, and R. R. Alfano, "Second-harmonic tomography of tissues," Opt. Lett. **22,** 1323–1325 (1997).
10. Barry R. Masters, Andres Kriete, and Jorg Kukulies, "Ultraviolet confocal fluorescence microscopy of the invitro cornea-redox metabolic imaging," Appl. Opt. **32,** 592–596 (1993).
11. S. G. Demos and R. R. Alfano, "Optical polarization imaging," Appl. Opt. **36,** 150–155 (1997).
12. S. G. Demos, H. B. Radousky, and R. R. Alfano, "Deep surface imaging in tissue using spectral and polarization filtering," Opt. Express **7,** 23–28 (2000).
13. W. S. Bickel, J. F. Davidson, D. R. Huffman, and R. Kilkson, "Application of polarization effects in light scattering: a new

biophysical tool," Proc. Natl. Acad. Sci. USA **73,** 486–490 (1976).
14. K. Sokolov, R. Drezek, K. Gossage, and R. Richards-Kortum, "Reflectance spectroscopy with polarized light: is it sensitive to cellular and nuclear morphology," Opt. Express **5,** 302–317 (1999).
15. M. Dogariu and T. Asakura, "Photon path length distribution from polarized backscattering in random media," Opt. Eng. **35,** 2234 (1996).
16. B. D. Cameron, M. J. Rakovic, M. Mehrubeoglu, G. W. Kattawar, S. Rastegar, L. V. Wang, and G. L. Coté, "Measurement and calculation of the two-dimensional backscattering Mueller matrix of a turbid medium," Opt. Lett. **23,** 485–487 (1998).
17. B. D. Cameron, M. J. Rakovic, M. Mehrubeoglu, G. W. Kattawar, S. Rastegar, L. V. Wang, and G. L. Coté, "Measurement and calculation of the two-dimensional backscattering Mueller matrix of a turbid medium: errata," Opt. Lett. **23,** 1630–1630 (1998).
18. M. J. Rakovic, G. W. Kattawar, M. Mehrubeoglu, B. D. Cameron, S. Rastegar, L. V. Wang, and G. L. Coté, "Light backscattering polarization patterns from turbid media: theory and experiment," Appl. Opt. **38,** 3399–3408 (1999).
19. A. H. Hielscher, J. R. Mourant, and I. J. Bigio, "Influence of particle size and concentration on the diffuse backscattering of polarized light from tissue phantoms and biological cell suspensions," Appl. Opt. **36,** 125–135 (1997).
20. S. L. Jacques, M. Ostemeyer, L. V. Wang, and D. Stephens, "Polarized light transmission through skin using video reflectometry: toward optical tomography of superficial tissue layers," in Proc. SPIE **2671,** 199–210 (1996).
21. S. L. Jacques and K. Lee, "Imaging tissues with a polarized light video camera," in Proc. SPIE **3863,** 68–74 (1999).
22. S. L. Jacques and R. J. Ramella-Roman, "Propagation of polarized light beams through biological tissues," in Proc. SPIE **3914,** 345 (2000).
23. S. G. Demos and R. R. Alfano, "Optical polarization imaging," Appl. Opt. **36,** 150–155 (1997).
24. A. H. Hielscher, A. A. Eick, J. R. Mourant, D. Shen, J. P. Freyer, and I. J. Bigio, "Diffuse backscattering Mueller matrices of highly scattering media," Opt. Express **1,** 441–453 (1997).
25. F. Delplancke, "Automated high-speed Mueller matrix scatterometer," Appl. Opt. **36,** 5388–5395 (1997).
26. J. M. Bueno, "Polarimetry using liquid-crystal variable retarders: theory and calibration," J. Opt. A **2,** 216–222 (2000).
27. J. L. Pezzaniti and R. A. Chipman, "Mueller matrix imaging polarimetry," Opt. Eng. **34,** 1558–1568 (1995).
28. M. Mujat and A. Dogariu, "Real-time measurement of the polarization transfer function," Appl. Opt. **40,** 34–44 (2001).
29. S. Y. Lu and R. A. Chipman, "Interpretation of Mueller matrices based on polar decomposition," J. Opt. Soc. Am. A **13,** 1–8 (1996).
30. J. J. Gil and E. Bernabeu, "Obtainment of the polarizing and retardation parameters of a non-depolarizing optical system from the polar decomposition of its Mueller matrix," Optik (Stuttgart) **76,** 67–71 (1987).
31. R. Sridhar and R. Simon, "Normal form for Mueller matrices in polarization optics," J. Mod. Opt. **41,** 1903–1915 (1994).
32. G. L. Liu, Y. Li, and B. D. Cameron, "Polarization-based optical imaging and processing techniques with application to cancer diagnostics," in *International Biomedical Optics Conference,* Proc. SPIE **4617,** 208–220 (2002).
33. M. H. Smith, A Lompado, and P. Burke, "Mueller matrix imaging polarimetry in dermatology," in Proc. SPIE **3911,** 210–216 (2000).
34. J. S. Baba, J. R. Chung, A. H. DeLaughter, B. D. Cameron, and G. L. Cote, "Development and calibration of an automated Mueller matrix polarization imaging system," J. Biomed. Opt. **7,** 341–349 (2002).
35. L. Wang and S. Jacques, "Non-invasive detection of skin cancers by measuring optical properties of tissue," in Proc. SPIE **2395,** 548–558 (1995).
36. R. M. A. Azzam and N. M. Bashara, *Ellipsometry and Polarized Light* (Elseveir, 1987).
37. S. Y. Lu and R. A. Chipman, "Interpretation of Mueller matrices based on polar decomposition," J. Opt. Soc. Am. A **13,** 1–8 (1996).
38. J. J. Salley, "Experimental carcinogenesis in the cheek pouch of the Syrian hamster," J. Dent. Res. **33,** 253–262 (1954).
39. A. Ebihara, T. B. Krasieva, L. H. Liaw, S. Fago, D. Messadi, K. Osann, and P. Wilder-Smith, "Detection and diagnosis of oral cancer by light-induced fluorescence," Lasers Surg. Med. **32,** 17–24 (2004).
40. P. Wilder-Smith, A. Ebihara, L. H. Liaw, T. B. Krasieva, and D. Messadi, "Detection of dysplasia and malignancy in oral mucosa using autofluorescence," Lasers Surg. Med. **12,** 264 (2000).